ANALYSIS OF AN OSCILLATING PLATE COUPLED WITH FLUID

By

Michael Joseph Nash

RECOMMENDED:

Dr. Gang Sheng

Dr. Chuen-Sen Lin

Dr. Jifeng Peng, Advisory Committee Chair

Dr. Rorik Peterson
Chair, Department of Mechanical Engineering

APPROVED:

Dr. Douglas Goering
Dean, College of Engineering and Mines

Dr. John Eichelberger
Dean of the Graduate School

17 December 2013
Date

ANALYSIS OF AN OSCILLATING PLATE COUPLED WITH FLUID

A

THESIS

Presented to the Faculty

of the University of Alaska Fairbanks

in Partial Fulfillment of the Requirements

for the Degree of

MASTER OF SCIENCE

By

Michael J. Nash, B.S.

Fairbanks, Alaska

December 2013

Abstract

The mechanical vibration of an oscillating cantilever plate is studied to determine the interaction of a plate coupled with air and with water. Experimental data was collected and analyzed using multiple methods including Fast Fourier Transform, wavelet analysis, and the Hilbert-Huang Transform (HHT) to characterize the behavior of the plate. The HHT is able to process nonlinear and nonstationary signals and provides more meaningful information compared to the traditionally used Fourier transform for similar applications. The HHT was found to be appropriate and more descriptive for the analysis of coupled fluid-structure systems. Digital Particle Image Velocimetry (DPIV) was also used to analyze the circulation and energy transferred to the fluid.

Table of Contents

Page

List of Tables

Page

List of Figures

Page

Chapter 1 Introduction

Fluid structure interactions are of interest in many applications, ranging from marine structures and vessels to the propulsion of fish and other swimming animals. The response of the structure to the flow of the surrounding fluid is also of interest in energy harvesting. Many methods have been developed for studying the interaction of the fluid and structure.

Experiments were performed by Lindholm, Kana, Chu, and Abramson [1] with plates of different aspect ratios and thickness ratios, oscillating partially and fully submerged in water. Added mass correction factors were developed for the first six modes of vibrations. Fu and Price [2] used a linear hydroelasticity theory and a finite element method to calculate generalized added mass and damping coefficients which supported the conclusions found in the experimental work of Lindholm et al.

Keulegan and Carpenter [3] performed a series of experiments measuring the inertia, and drag coefficients for cylinders and plates coupled with water subjected to a standing wave. In this application they determined that the inertia and drag coefficients, as well as the force on the structure, are correlated to a nondimensional period parameter. This period parameter is a function of: the maximum intensity of the sinusoidal current, the period of the wave, and the length scale of the cylinder or plate.

Many methods of employing numerical solutions have been developed [4, 5]. Each of these methods determined the dry and wet natural frequencies of oscillating plates, by employing boundary integral equations, and added mass formulations. These numerical results compared well with results from [1] and [2], with an error of 5% in air,

and 10% in water. It was found that the natural frequency decreases with increasing aspect ratio, and increases with increasing thickness ratio.

Other numerical methods have been developed which couple a computational fluid dynamics solver with a computational solid dynamics solver to simultaneously solve the equation of motion and the Navier-Stokes equation. These methods have proved to be very time consuming. Münch, Ausoni, Braun, Farhat, and Avellan [6] avoided this method, and instead performed modeling of an oscillating hydrofoil subjected to a linearized hydrodynamic load. A Hybrid Coupling method has been developed by Young, Chae, and Akcabay [7] where an analytical approximation of the hydroelastic forces is embedded in the solution process to obtain better initial estimates of the displacements. The Hybrid Coupling algorithm is designed for the coupling of general viscous flow solvers with structural solvers to account for nonlinear viscous fluid structure interactions.

As a direct application for marine vessels, Klaka, Penrose, Horsley, and Renilson [8] performed tests on plates undergoing displacement amplitudes modeled after sailing yacht keels. Tests were performed on scaled plates with oscillation amplitudes of 7.5 to 20 degrees. They determined that the total roll moment, roll inertia, roll drag, and sway force coefficients showed an inverse square root relationship to aspect ratio, and a very weak dependence on oscillation frequency and angle amplitude.

The flexibility of the plate has a large influence on the behavior of the system. Testing plates with variable chordwise rigidity, Barannyk, Buckham, and Oshkai [9] performed experiments with a heaving and pitching plate in the thrust producing regime.

It was found that the more flexible plate achieved the highest propulsive efficiency and thrust.

The flow induced vibration of structures is a common phenomenon. Vortex induced vibrations in particular have received a great amount of study. They occur in many engineering situations, and it is necessary to understand the interaction between the fluid and the structure. The vibrations may be of such magnitude to cause fatigue or failure of structures, as well as be employed for energy harvesting [10]. The fluid response and behavior is well understood for certain geometries such as cylinders; however, the fluid-structure interactions require further study as a dynamic system. Some success has been achieved in the application of plates in flow as energy harvesting devices. These plates undergo flutter and energy is transferred from the fluid to the vibration of the plates. This flutter-mill has been shown to be an effective method of energy harvesting and is compared with the output of a horizontal axis wind turbine [11].

Most of the previous work has been concerned with determining the resonant frequencies of plates in air and water. It was found that the resonant frequencies were largely dependent on the aspect ratio and thickness ratio of the plate being tested. Empirical and numerical solutions have been developed for determining an added mass correction factor based on the vibration mode, as well as solutions for the coefficients of roll, drag, inertia, and sway forces. These solutions are useful but do not fully describe the response of a plate coupled with water. Many researchers have simply assumed a linear response of the plate; however, this assumption may not be valid. This study will

compare the results and appropriateness of a few methods for analyzing the mechanical vibrations of flat plates in air and water.

Chapter 2 Method

2.1 Equipment Setup

The experiments were conducted using plates of aspect ratio (AR) 7. The thin rectangular plates were secured to the supporting framework by a spacer and screws. The dimensions of the plate are 177.8 x 25.4 x 1.59 mm for an AR of 7. Three materials were used for the plates; their mechanical properties are listed in Table 2.1.

Table 2.1: Mechanical Properties of Materials

	1018 Low Carbon Steel	6061 Aluminum	Nylon 6/6
Density (kg/m^3)	7833	2712	1150
Modulus of Elasticity (GPa)	201	69	3
Yield Strength (MPa)	305	256	45
Tensile Strength (MPa)	417	277	82

Experiments were performed with the plates in air and then in water. The plates were submerged in a 1.52 x 0.6 x 0.6 m water tank. The plate is 0.2 m from the sides and bottom of the tank, and 0.2 meters below the free surface of the water. A schematic of the equipment is included in Figure 2.1.

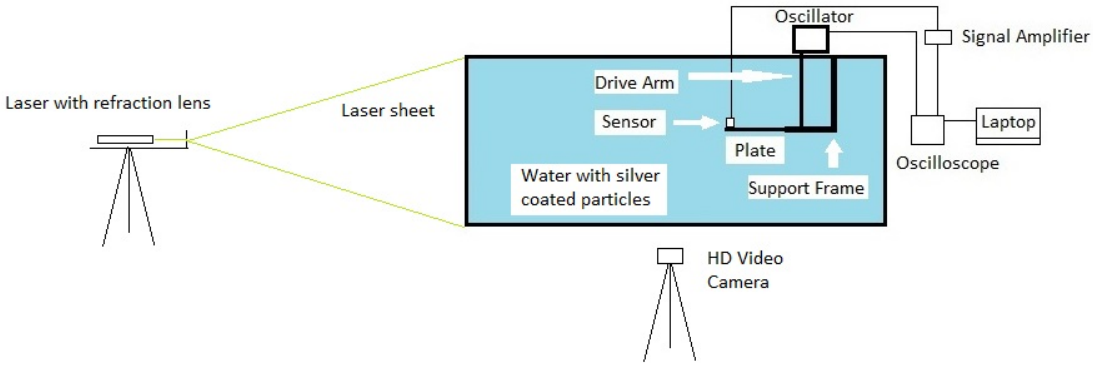

Figure 2.1: Equipment Setup

2.2 Data Collection Parameters

Two sets of data were collected for each experimental run. One channel of data was used for the accelerometer, and one channel for the output of the oscillator. The sensor used was a PCB Piezotronics Model 352B30 accelerometer. The oscillator used was a Cenco Physics Vibration Generator. The signal amplifier used was a PCB Piezotronics Model 482C sensor signal conditioner. The oscilloscope used was a Tektronix TDS 3054B. The software used to collect the data was Tektronix e*Scope™. The camcorder used was a Canon XA10 HD Professional Camcorder with a 1920 x 1080 complementary metal-oxide semiconductor sensor. Illuminating the particles is a Hercules series laser manufactured by Laserglow Technologies. The 500 mW green laser emits a 532nm green light which is refracted through a lens to form a vertical plane through the tank. The silver coated hollow glass beads have an average size of 13 micrometers.

2.3 Analysis Methods

Multiple methods have been developed to process and analyze discrete digital signals. One of the most widely used methods is the Discrete Fourier Transform. This method is very useful and well developed; however, it is limited in its application.

2.3.1 Fast Fourier Transform

A useful tool for evaluating signals is the Fourier Transform. It is very convenient as it allows a signal to be represented as a linear combination of simple sine and cosine functions. The Fourier Transform and Fast Fourier Transform (FFT) have been used with great success in representing discrete signals in mathematical terms. The FFT is limited though by two assumptions: that the response is linear, and time invariant [12]. Vortex induced vibrations are inherently nonlinear [10] which makes the FFT ill suited for analyzing these signals with great accuracy.

2.3.2 Wavelet

The wavelet analysis is a method used to determine the characteristics of a signal in time and space. The FFT assumes a linear and stationary signal, and it does not describe the time when events have occurred within the sampling period. The wavelet analysis allows for these events to be reported and recognized. The time and duration of these events may also be determined by the wavelet analysis [13]. The sampled signal is decomposed as a summation of a single base signal which has varying amplitude, and varying distribution in time. By summing the signals at each scale, the original signal

may be reproduced. The benefit of the wavelet analysis is that it describes the frequencies present throughout the entire sampling period.

2.3.3 Hilbert-Huang Transform

The HHT is able to analyze data from nonlinear and nonstationary processes. This is accomplished through the results of empirical mode decomposition (EMD), and the Hilbert spectral analysis (HSA) methods, as introduced by Huang, and Attoh-Okine [14]. EMD reduces any given data into a collection of intrinsic mode functions (IMF) by an iterative sifting process, to which the HSA can be applied. An IMF is any function with the same number of extrema and zero crossings, with its envelopes defined by all the local maxima and minima, being symmetric with respect to zero.

The EMD is obtained in the following steps:

1. For any given data $z(t)$, we identify the local extrema and then connect all the local maxima by a cubic spline line as the upper envelope. The procedure is repeated for the local minima to produce the lower envelope.
2. The upper and lower envelopes should contain all the data between them. Their mean is designated as $m_1(t)$, and the difference between the data and $m_1(t)$ is the first proto-IMF (PIMF) component, $h_1(t) = z(t) - m_1(t)$.
3. This PIMF $h_1(t)$ should meet the definition of an IMF, but it may not. If it does not, the sifting process must be repeated as many times as necessary to satisfy the definition of an IMF. In the subsequent sifting process steps $h_1(t)$ is treated as the data, then $h_{11}(t) = h_1(t) - m_{11}(t)$. Where $m_{11}(t)$ is the

mean of the upper and lower envelops of $h_1(t)$. This process can be repeated up to k times, then $h_{1k}(t)$ is given by $h_{1k}(t) = h_{1(k\text{-}1)}(t) - m_{1k}(t)$.

4. Two stoppage criteria have been proposed which determine the number of sifting steps required to produce an IMF.
    a. A sum of the difference (SD) is defined where

$$SD = \frac{\sum_{t=0}^{T} \left| h_{k-1}(t) - h_k(t) \right|^2}{\sum_{t=o}^{T} h_{k-1}^2(t)} \tag{1}$$

    b. The S-number is defined as the number of consecutive siftings when the numbers of zero-crossings and extrema are equal or at most differing by one.
5. When the resulting function satisfies either of the criteria, this component is designated as the first IMF, $c_1(t)$. The remainder is defined as the difference of the original data and the first IMF as $z(t) - c_1(t) = r_1(t)$.
6. The remainder $r_1(t)$ is treated as new data and subjected to the sifting process just described for j iterations, where $r_1(t) - c_2(t) = r_2(t)$, and $r_{n\text{-}1}(t) - c_n(t) = r_n(t)$.
7. By summing all the IMFs, we obtain a decomposition of the data into n IMF modes, and a residue r_n, which can be a constant, a monotonic mean trend, or a curve having only one extremum.

$$z(t) = \sum_{j=1}^{n} c_j(t) + r_n(t) \tag{2}$$

The Hilbert transform can now be applied to each IMF component $c_j(t)$ and the instantaneous frequency can be computed as the derivative of the phase function.

$$H[c_j(t)] = \frac{1}{\pi}\int_{-\infty}^{\infty}\frac{c_j(t)}{t-\tau}d\tau \tag{3}$$

The Hilbert transform is combined with the IMF to form a complex signal $Z_j(t)$.

$$Z_j(t) = c_j(t) + iH[c_j(t)] = a_j(t)e^{i\varphi(t)} \tag{4}$$

Where $a_j(t)$ is the instantaneous amplitude of $Z_j(t)$, and $\varphi_j(t)$ is the instantaneous phase.

$$a_j(t) = \sqrt{[c_j(t)]^2 + H[c_j(t)]} \tag{5}$$

$$\varphi_j(t) = \arctan\{H[c_j(t)]/c_j(t)\} \tag{6}$$

The instantaneous frequency $\omega(t)$ is defined as the time derivative of the instantaneous phase $\varphi(t)$.

$$\omega(t) = \frac{d\varphi(t)}{dt} \tag{7}$$

The original signal $z(t)$ may now be expressed as

$$z(t) = \sum_{j=1}^{n} a_j(t)\exp\left[i\int \omega_j(t)dt\right] \tag{8}$$

2.3.4 Digital Particle Image Velocimetry

There are several techniques available for visualizing the flow of fluids. Digital Particle Image Velocimetry (DPIV) is a method which provides qualitative and quantitative information about the flow. This method includes placing tracer elements into the fluid. The flow is filmed and the video is separated into individual frames.

Software is used to trace the particles as they move frame by frame. By specifying a physical scale for each frame and the time between frames, the position and velocity of each particle may be computed. Once the velocity is known, the vorticity may be computed as a line integral of the velocity. The velocity and vorticity information can be used to observe and quantify the flow around objects.

Chapter 3 Experiment

3.1 Design of Experiment

Experiments were conducted at different forcing amplitudes and frequencies as listed in Table 3.1. The forcing amplitude in Table 3.1 was measured from the vibration generator and used as a measure of the displacement amplitude. A full factorial design was used such that data was recorded for every combination of amplitude, frequency, plate material, and fluid. This factorial of 3 amplitude, 3 frequencies, 3 materials and 2 fluids resulted in 54 experiments. Two sets of data were collected for each experiment conducted. The two sets of data were used for comparison to determine repeatability of the experiment.

Table 3.1: Input Parameters

Amplitude (Volts)	Frequency (Hz)
4	15
4.5	22.5
5	30

These parameters were chosen because they each showed a wide range of response and were well below the calculated natural frequencies of the plates as seen in Table 3.2. The equation for the natural frequency can be seen in equation 9, where k_{eq} is the equivalent spring rate of the plate, and m_{eq} is the equivalent mass of the plate.

$$\omega_n = \sqrt{\frac{k_{eq}}{m_{eq}}} \tag{9}$$

Table 3.2: Natural Frequencies

	1018 Low Carbon Steel	6061 Aluminum	Nylon 6/6
ω_n (Hz)	265	264	56

The test apparatus was placed on the tank in the same position for the dry and wet experiments. Every experiment was conducted for each dry material first. The tank was then filled with water and every wet experiment was conducted for each material. Each set of data was collected in succession. The sampling rate of 50 kHz was chosen because the data set provided detailed information without the files being overly large. With a steady and periodic forcing, the plate was expected to also respond in a periodic nature at frequencies very near to the forcing frequencies. The sampling period of .2 seconds was chosen because it was expected to provide three periods of oscillation at 15 Hz and 6 periods of oscillation at 30 Hz. Having multiple periods of the signal is useful for detecting errors in the gathered data or anomalies in the vibration.

To perform the DPIV analysis, a high definition video camera was used to record the fluid motion. The motion was visualized by the use of small visible particles which are suspended in the water, and illuminated with a planar laser sheet. These particles are easily visible under the laser's illumination. The use of hollow glass enables the particles to be neutrally buoyant in the fluid for long periods of time. Illuminating the particles is a laser, which is refracted through a lens to form a vertical plane through the tank, and perpendicular to the longitudinal axis of the plate. The single plane of light enables two dimensional flows to be observed.

Chapter 4 Analysis

4.1 Raw Data

The accelerometer and the oscillator output voltage signals. The data was collected as .txt files by the Tektronix software e*Scope™. These files each contained 10,000 data points including time and voltage measurements. The oscillator sampled the response of the plate at a rate of 50 kHz.

An abbreviated sample of the data is presented in Table 4.1, only 20 points are shown for clarity. Table 4.1 is the result of the dry steel plate forced at 4 V amplitude and 15 Hz. The first column is the time stamp, which begins at -0.1 s, and continues to 0.09998 s, the second column is the measured acceleration in volts output by the accelerometer.

Table 4.1: Selected Sample Data

Time (s)	Acceleration (V)
-0.09742	-0.0032
-0.09740	-0.0024
-0.09738	-0.0028
-0.09736	-0.0028
-0.09734	-0.0024
-0.09732	-0.0028
-0.09730	-0.0028
-0.09728	-0.0028
-0.09726	-0.0024
-0.09724	-0.0032
-0.09722	-0.0024
-0.09720	-0.0028
-0.09718	-0.0028

4.2 Data Analysis

Two MATLAB® m-files were used to analyze all the raw data. One m-file produced the following figures: waveform, FFT, and image scalogram of the wavelet analysis. To perform the HHT, a second m-file was used [15] to plot intrinsic mode functions and the instantaneous frequency of the response signal. This m-file produces figures of instantaneous frequency and multiple signal IMFs. These figures are used as the main tool for analysis.

To perform the DPIV analysis, the video recorded during the experiment must be analyzed. The process begins by using Adobe Premiere Pro to break down the video into many single frames. Once the video has been converted into many images, they were processed with the DPIV software. Matlab was used to take the velocity and vorticity data produced from the DPIV analysis to construct velocity and vorticity plots
These plots are useful to help visualize the flow interaction of the flow with the plates.

4.2.1 Waveform

The following figures show the waveform plots for each dry and wet material at 5 V and 15 Hz with a normalized amplitude of acceleration scale. Comparing these waveforms show the differences of the materials and how they respond as the plate is forced in both dry and wet conditions.

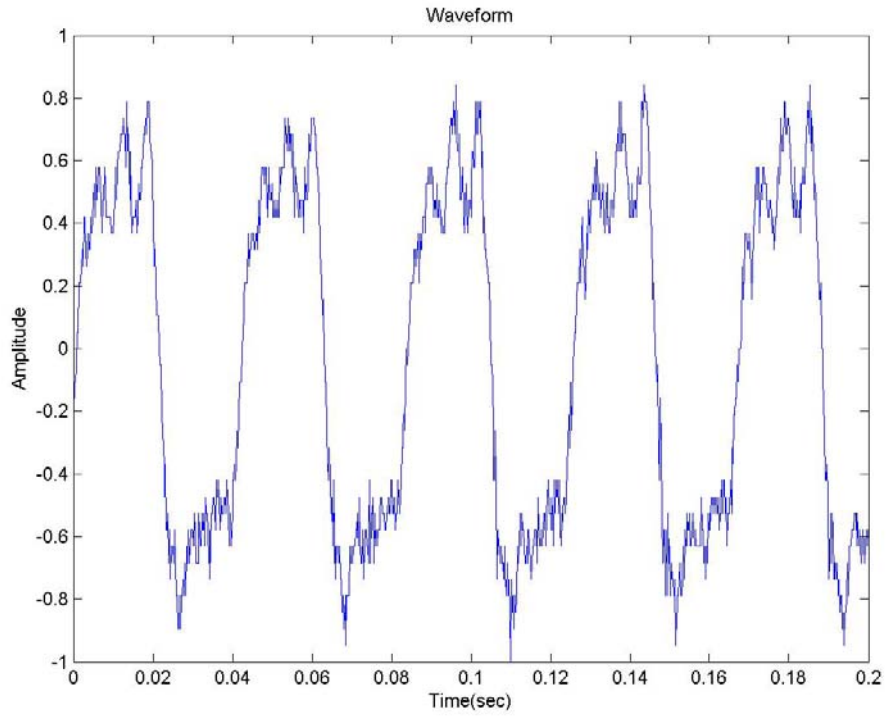

Figure 4.1: Air Steel 4.5 V 22.5 Hz Waveform

Figure 4.1 shows a very well described periodic signal with a frequency of approximately 17 Hz with some higher frequency components. A periodic response is also observed in Figure 4.2, but is complicated by other dominant signal components

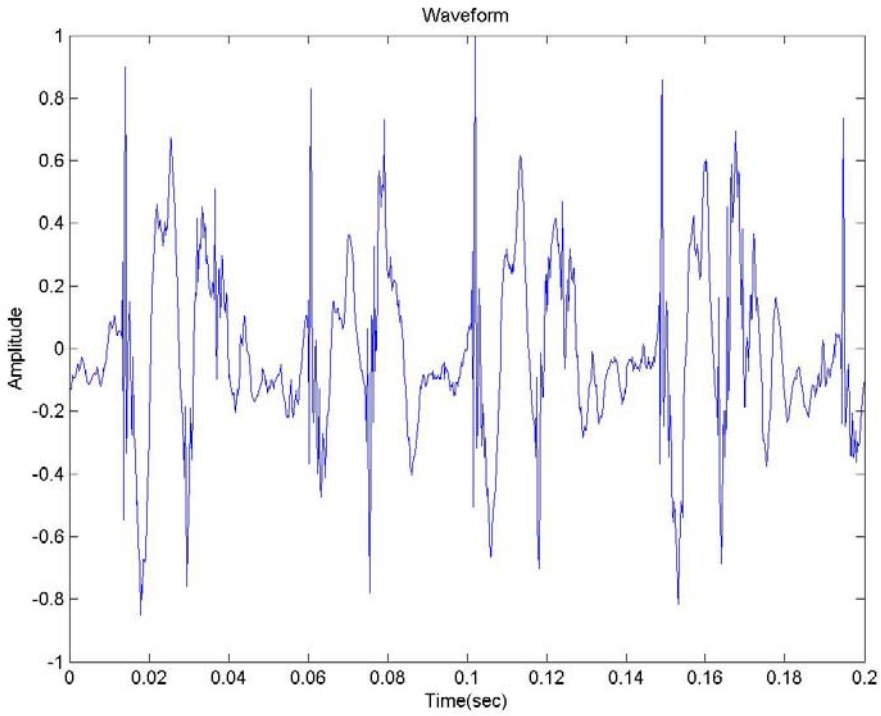

Figure 4.2: Water Steel 4.5 V 22.5 Hz Waveform

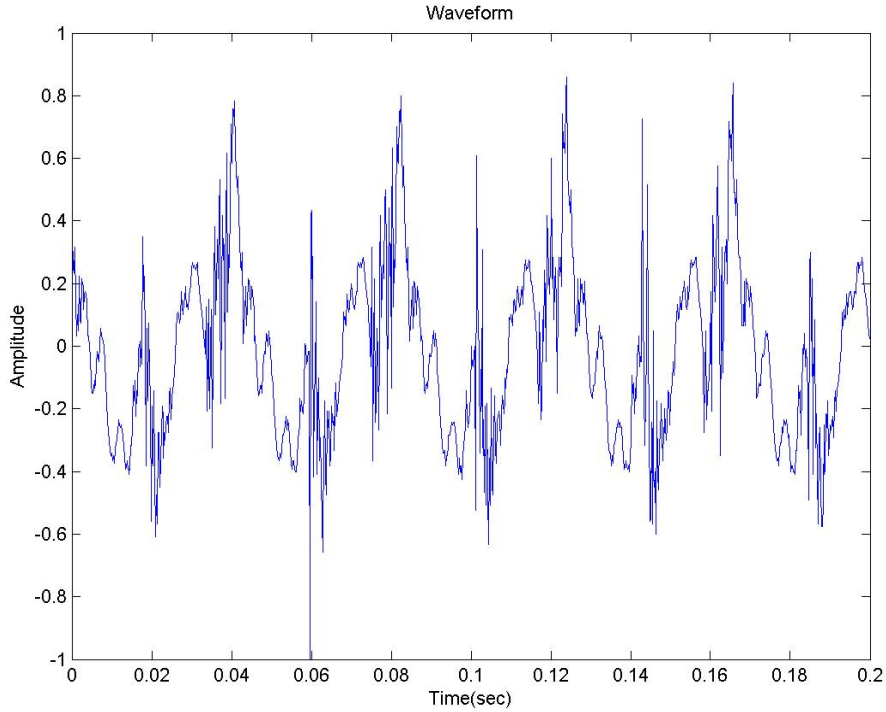

Figure 4.3: Air Aluminum 4.5 V 22.5 Hz Waveform

In contrast to the steel, Figure 4.3 describes more high frequency components than the dry steel of Figure 4.1, while Figure 4.4 describes multiple frequencies with near constant amplitude.

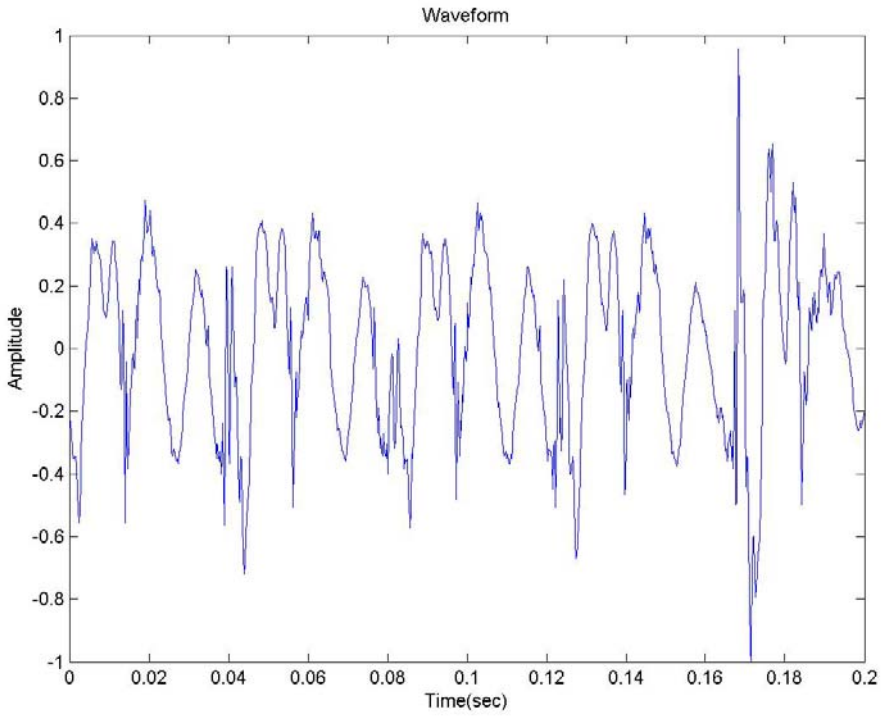

Figure 4.4: Water Aluminum 4.5 V 22.5 Hz Waveform

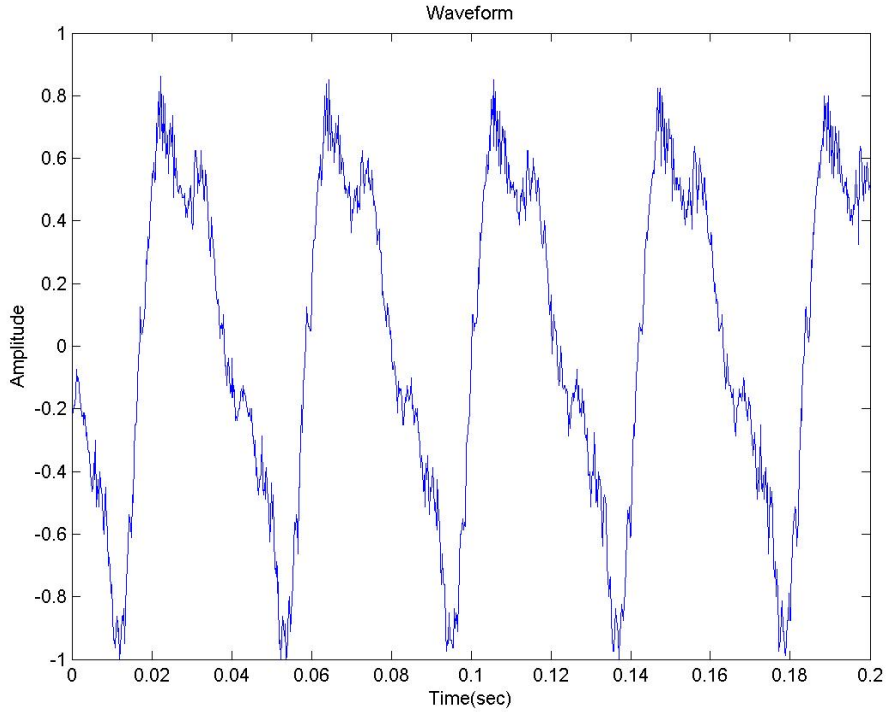

Figure 4.5: Air Nylon 4.5 V 22.5 Hz Waveform

Figure 4.5 describes a steady periodic signal dominated by a single frequency. Figure 4.6 is nearly identical in shape.

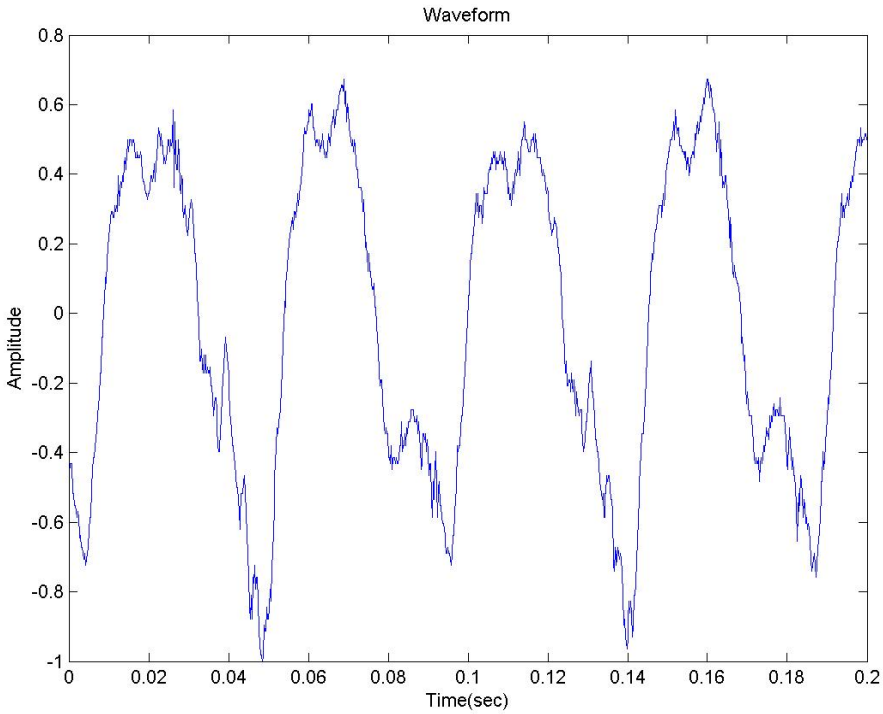

Figure 4.6: Water Nylon 4.5 V 22.5 Hz Waveform

4.2.2 Fast Fourier Transform

The FFT shows the frequencies present and their amplitudes which comprise the response signal. The following figures describe the frequencies present in the response of the plate are that of the forcing frequency 15 Hz. In the wet experiments, peaks were detected in multiples of the forcing frequency, such as 45 Hz, 67.5 Hz, and so on. Figures 4.7, 4.8, and 4.9, show the wet and dry data on the same plot to compare the effect of water.

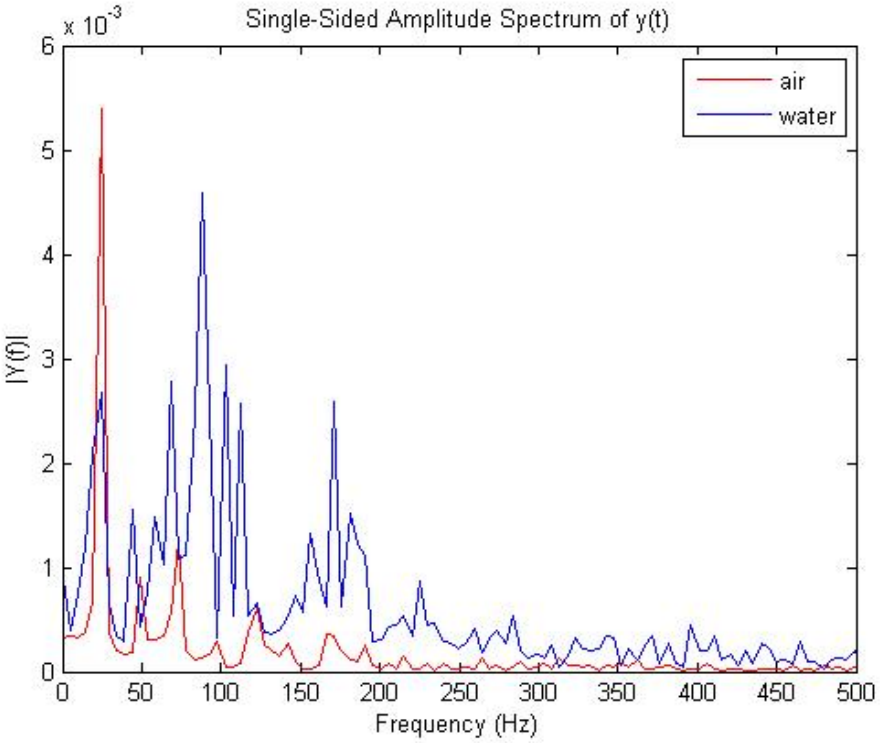

Figure 4.7: Steel 4.5 V 22.5 Hz FFT

Figure 4.7 shows the shift of frequencies from one peak at 15 Hz for the dry plate to having multiple dominate components at slightly higher frequencies. Figure 4.8 shows

similar frequency peaks as steel, but the multiple peaks have nearly the same amplitudes for the wet case.

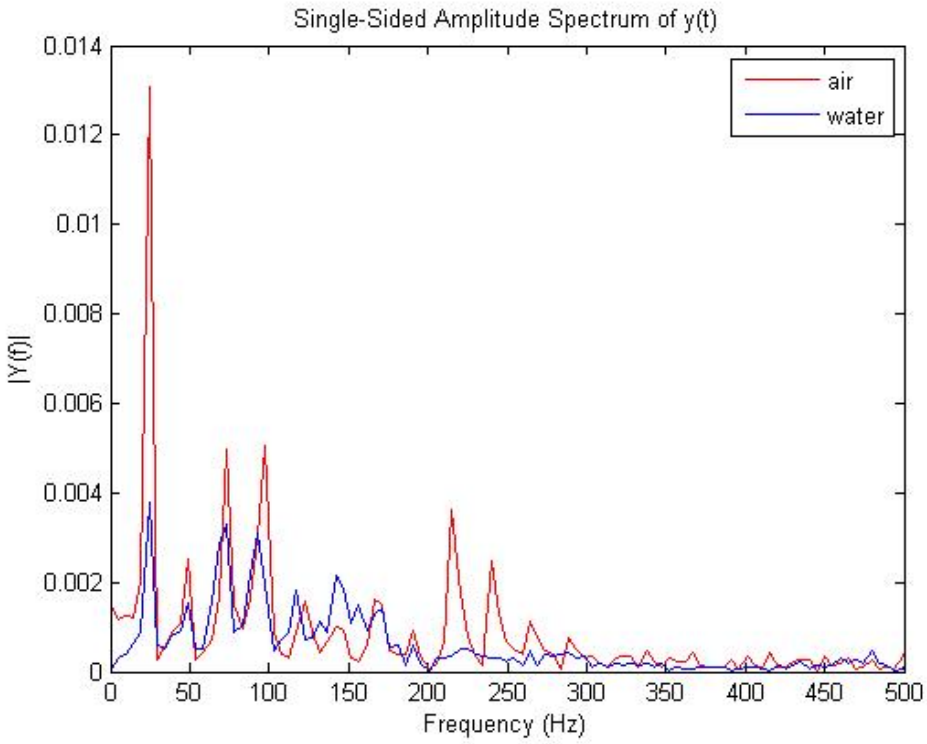

Figure 4.8: Aluminum 4.5 V 22.5 Hz FFT

Figure 4.9 describes a nearly identical transform for both the dry and wet nylon plates. In contrast to the other materials, the wet nylon shifted to slightly lower response frequencies with nearly the same amplitude as the dry nylon case.

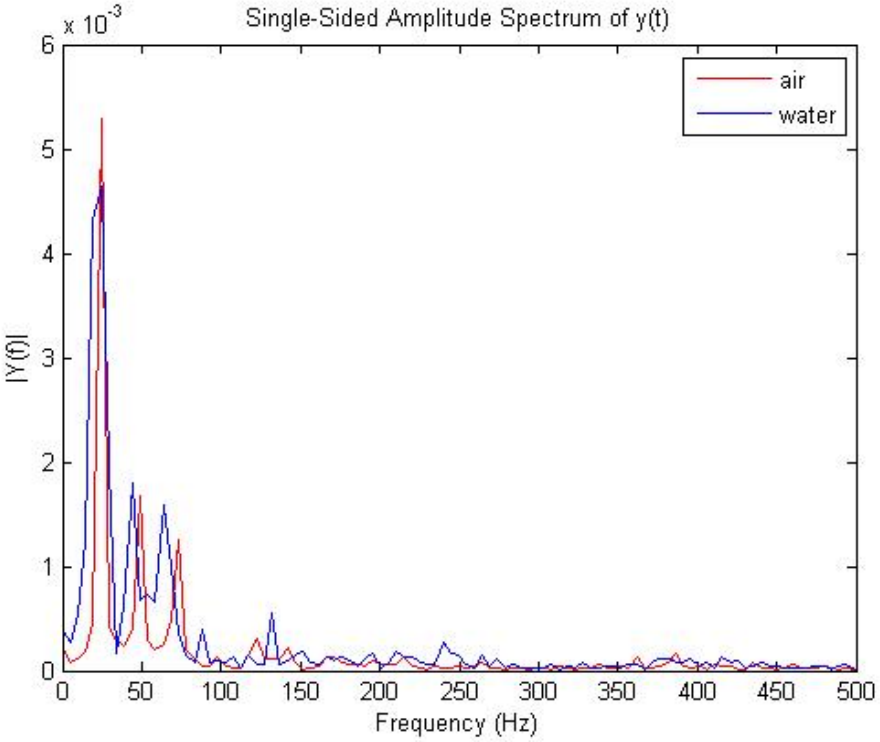

Figure 4.9: Nylon 4.5 V 22.5 Hz FFT

4.2.3 Wavelet

The following figures show how the frequency shifts occur for the dry and wet cases of each material. The image scalogram depicts a continuous spectrum of amplitudes in the dimensions of Scale a (frequency) and time. The scale is proportional to the frequency of the signal. A large decrease in Scale a is observed for the steel in Figures 4.10 and 4.11. Figures 4.12 and 4.13 for aluminum also show a very similar shift in frequency; however, with a slightly lesser shift in amplitude. Figures 4.14 and 4.15 show that the frequency shift is very slight, however, there was a detectable reduction in amplitude near the 500 time in Figure 4.15. The time and duration when this slight shift in amplitude takes place was not detected and reported by the FFT analysis in Figure 4.9. These wavelet analyses do add a dimension of time to the FFT.

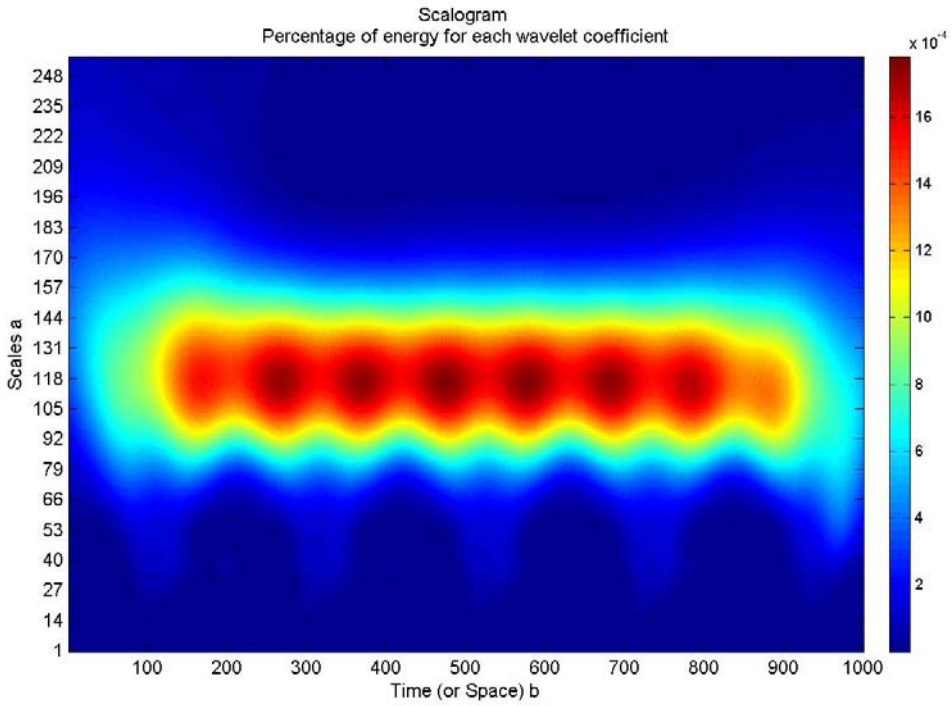

Figure 4.10: Air Steel 4.5 V 22.5 Hz Image Scalogram

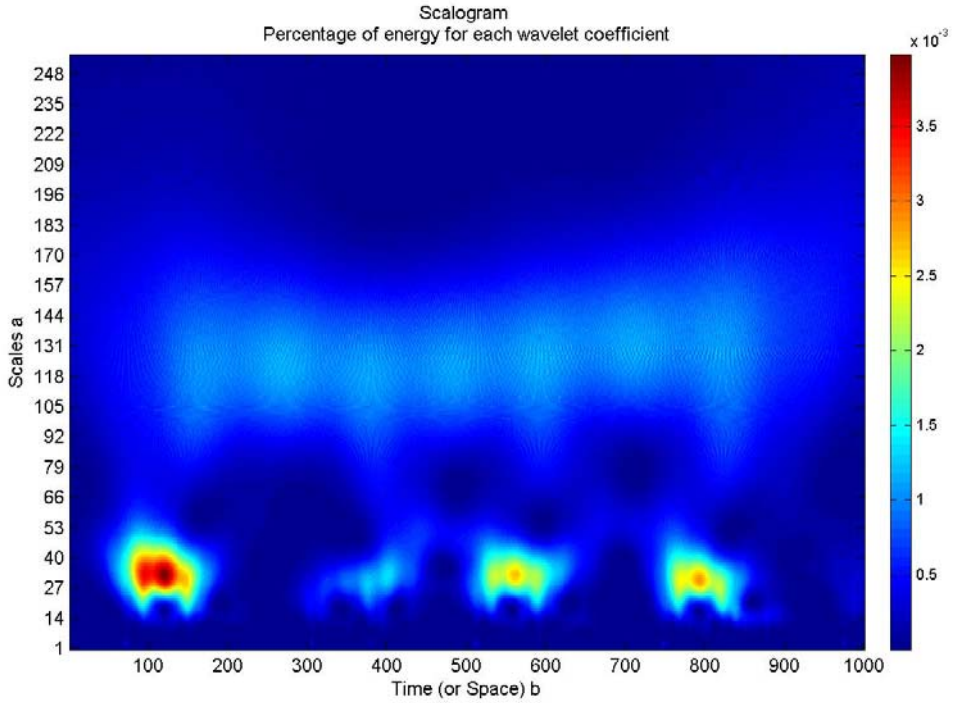

Figure 4.11: Water Steel 4.5 V 22.5 Hz Image Scalogram

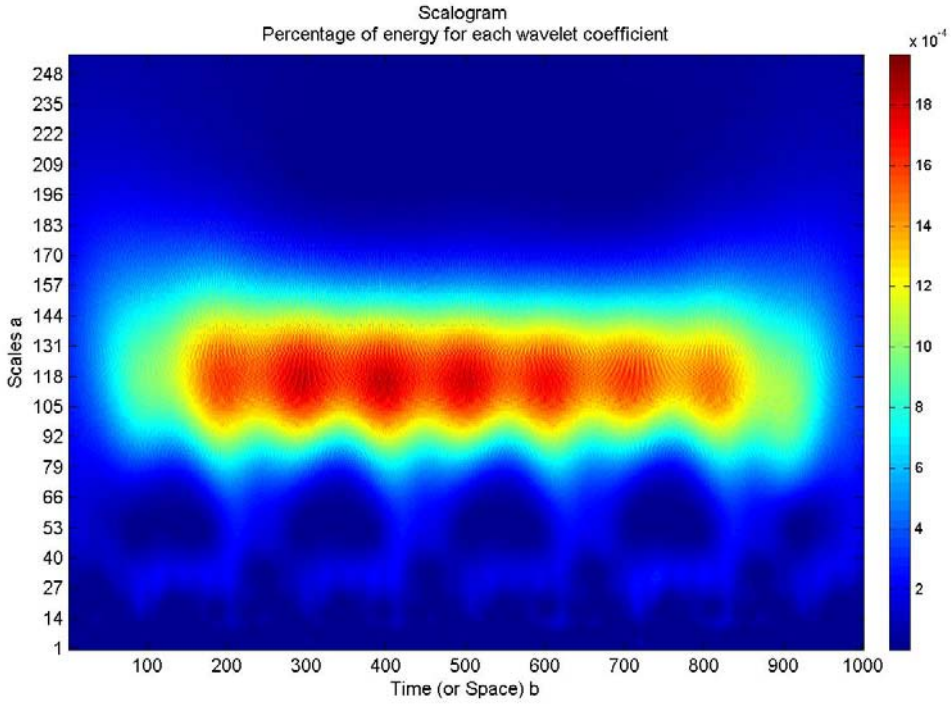

Figure 4.12: Air Aluminum 4.5 V 22.5 Hz Image Scalogram

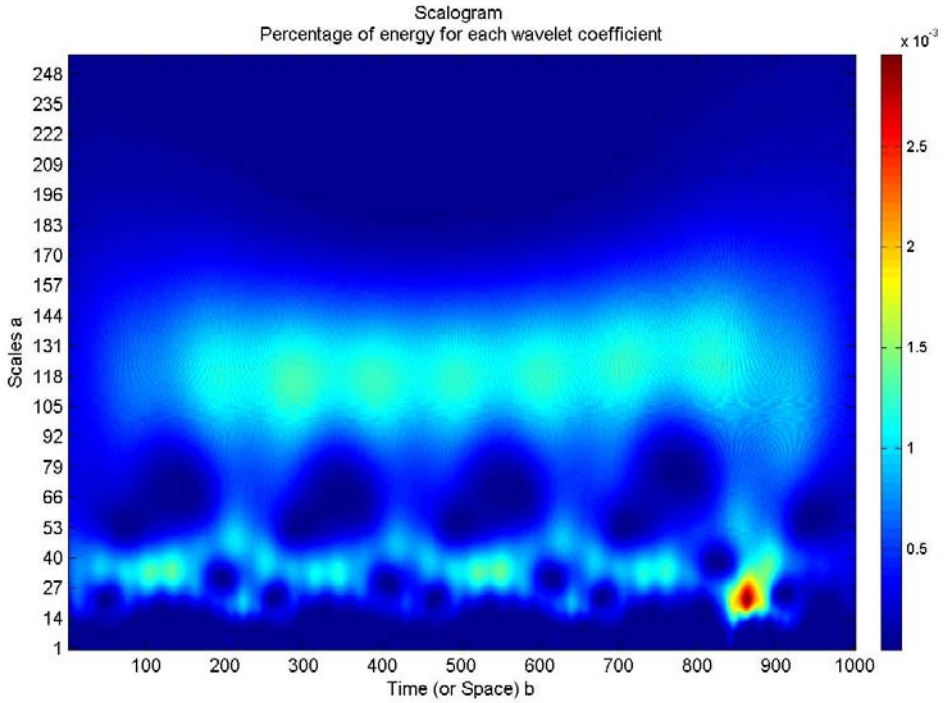

Figure 4.13: Water Aluminum 4.5 V 22.5 Hz Image Scalogram

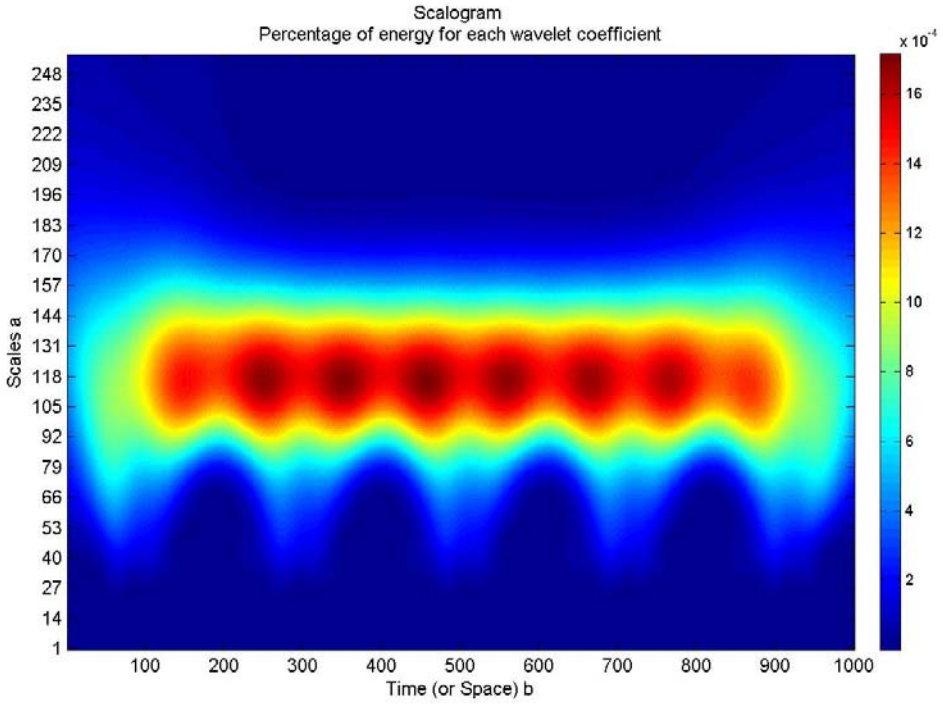

Figure 4.14: Air Nylon 4.5 V 22.5 Hz Image Scalogram

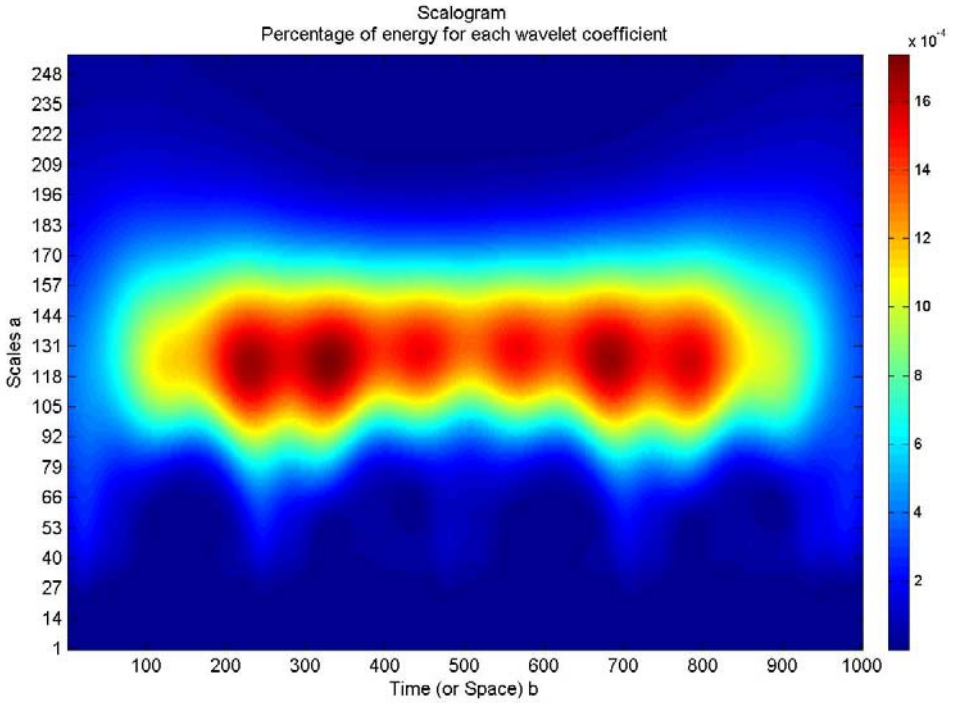

Figure 4.15: Water Nylon 4.5 V 22.5 Hz Image Scalogram

4.2.4 Hilbert-Huang Transform

The following plots show the results for dry and wet steel plates at 5 V and 15 Hz. Figures 4.16 and 4.20 describe the instantaneous frequencies for the dry and wet steel plate as defined by Equation 7 in Section 2.3.3. The range of instantaneous frequencies for the dry plate is from approximately 100 Hz to 450 Hz, whereas the wet plate experiences a considerably lower and much smaller range of only 100 Hz to 250 Hz.

Figure 4.17 includes the first 4 IMFs of the dry steel plate which depict very high frequency response components. These very high frequencies are most likely noise in the signal due to vibrations from the apparatus and do not provide much detail as to the

contributing frequencies. The IMFs in Figures 4.18 and 4.19 depict steady nearly constant frequency signals and a residue. This is in stark contrast to the IMFs for the wet steel plate in Figures 4.21 and 4.22, which include short duration period signals of high frequency.

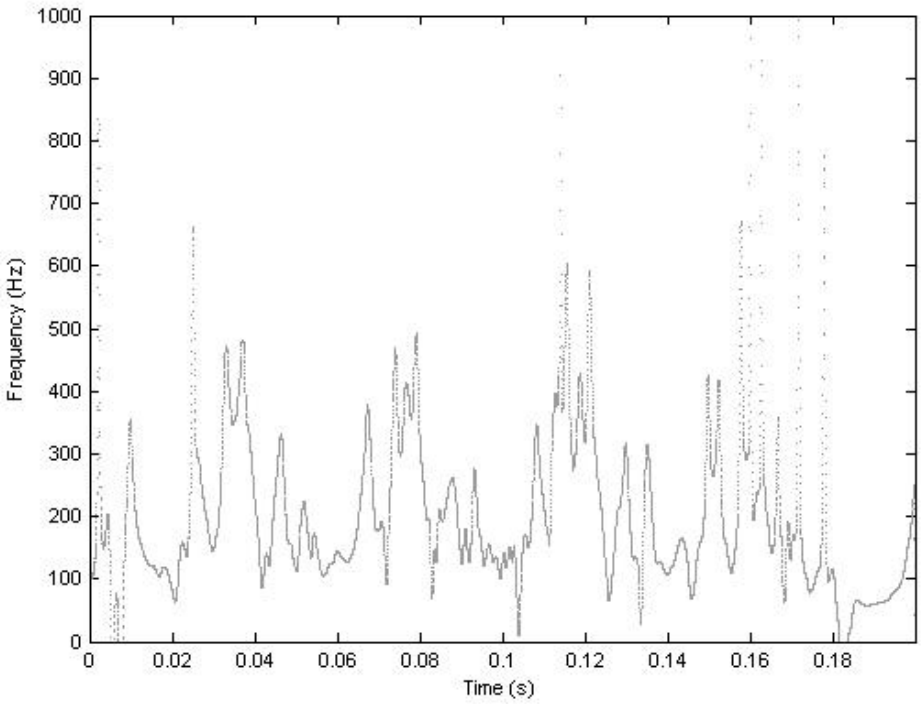

Figure 4.16: Air Steel 4.5 V 22.5 Hz Instantaneous Frequency

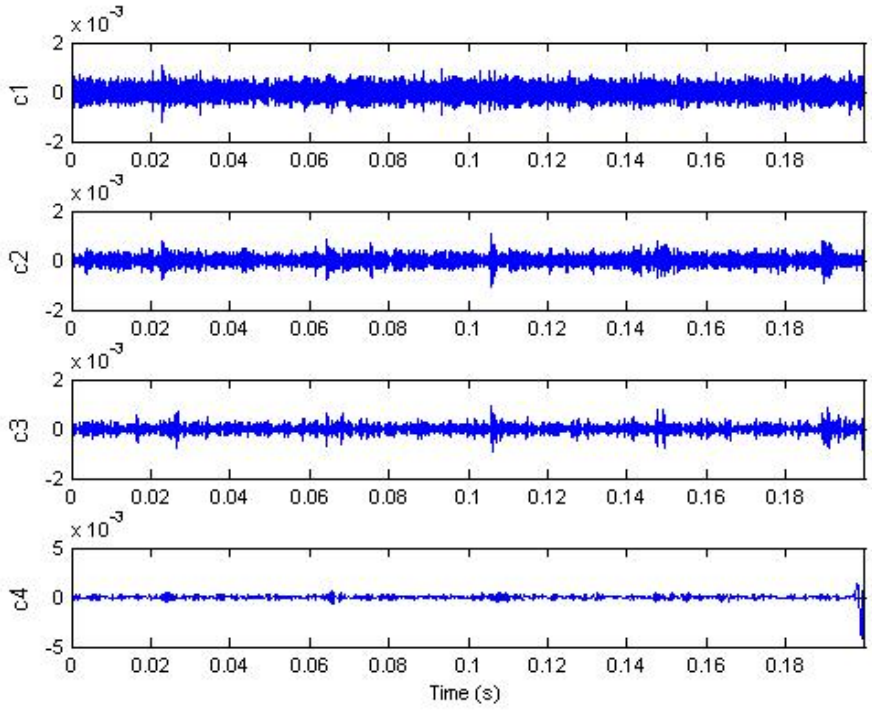

Figure 4.17: Air Steel 4.5 V 22.5 Hz IMF

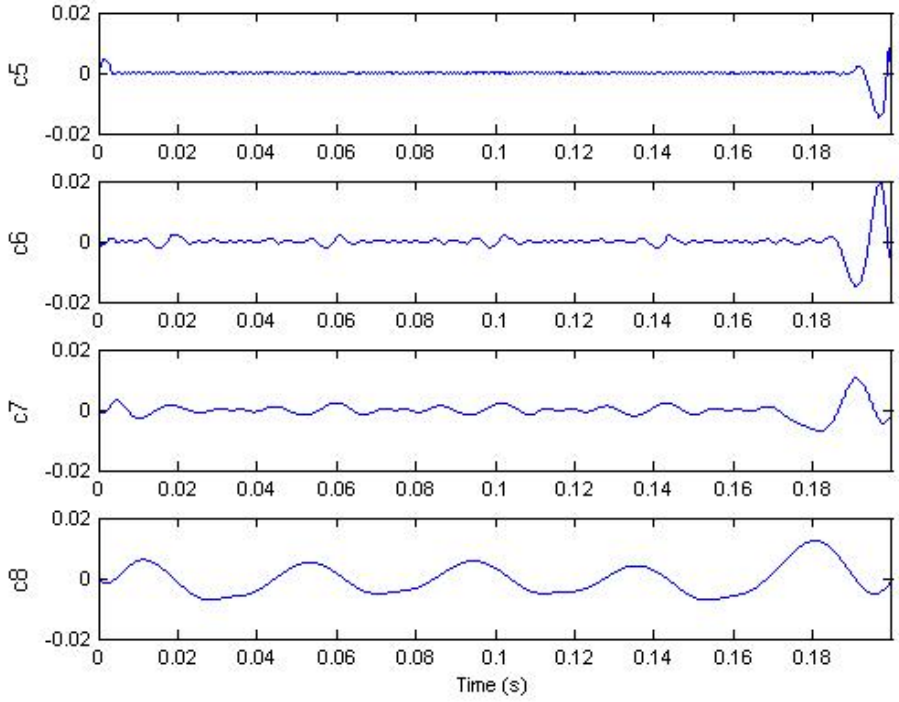

Figure 4.18: Air Steel 4.5 V 22.5 Hz IMF

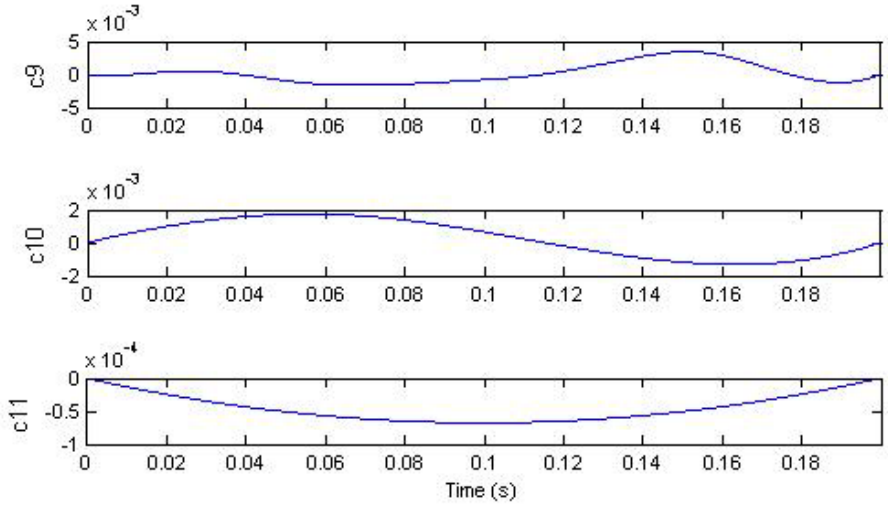

Figure 4.19: Air Steel 4.5 V 22.5 Hz IMF

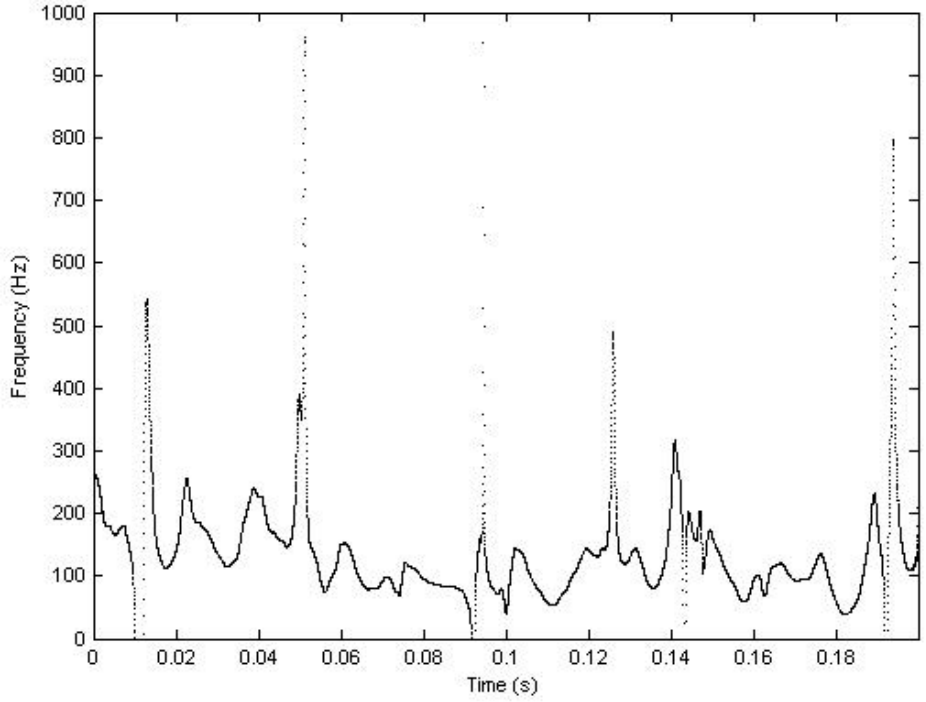

Figure 4.20: Water Steel 4.5 V 22.5 Hz Instantaneous Frequency

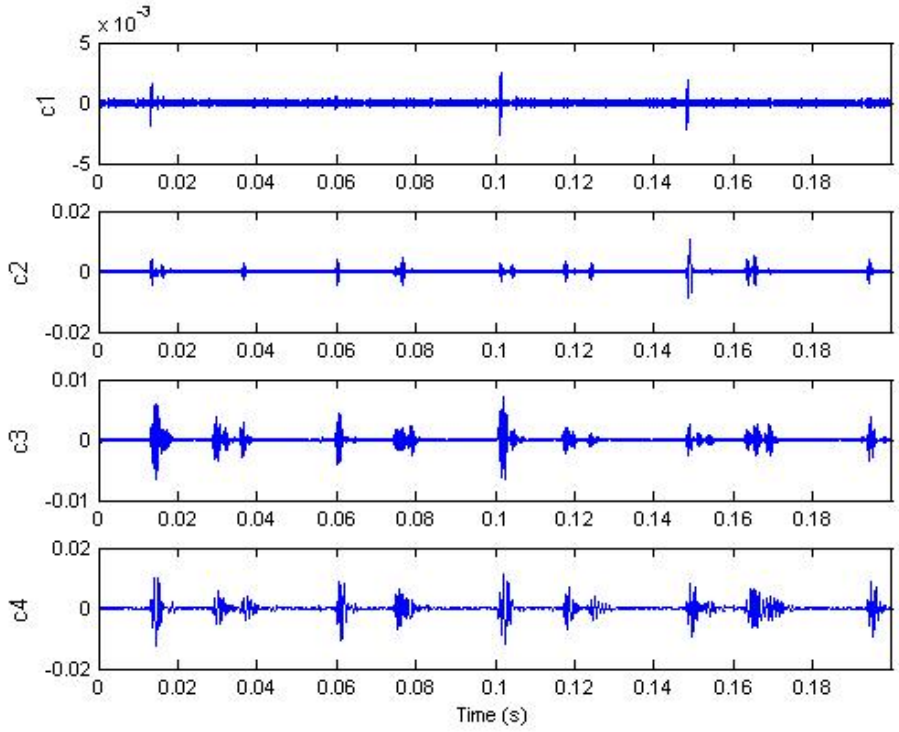

Figure 4.21: Water Steel 4.5 V 22.5 Hz IMF

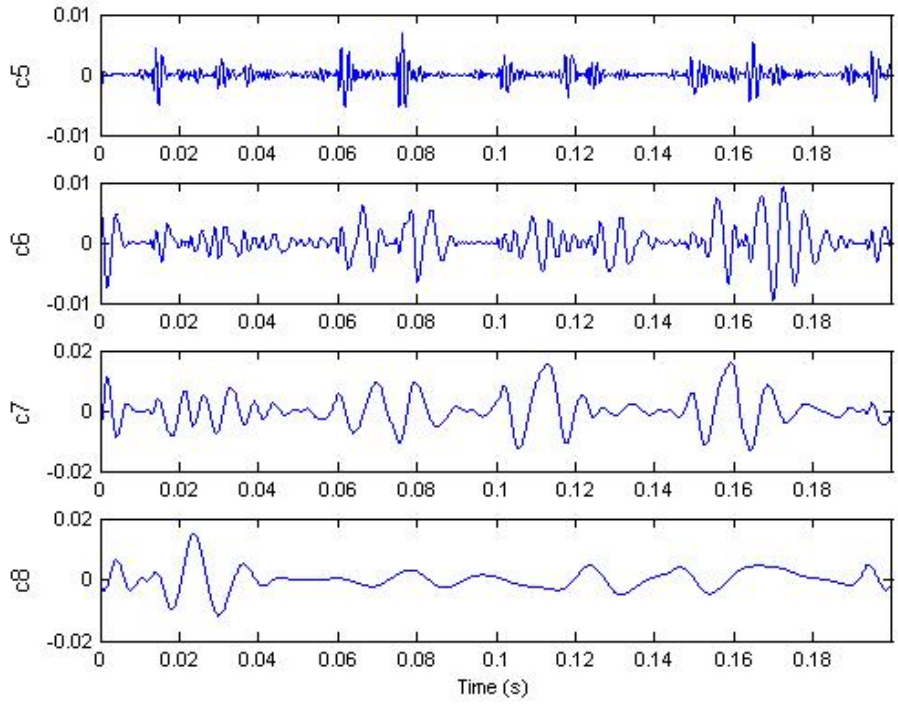

Figure 4.22: Water Steel 4.5 V 22.5 Hz IMF

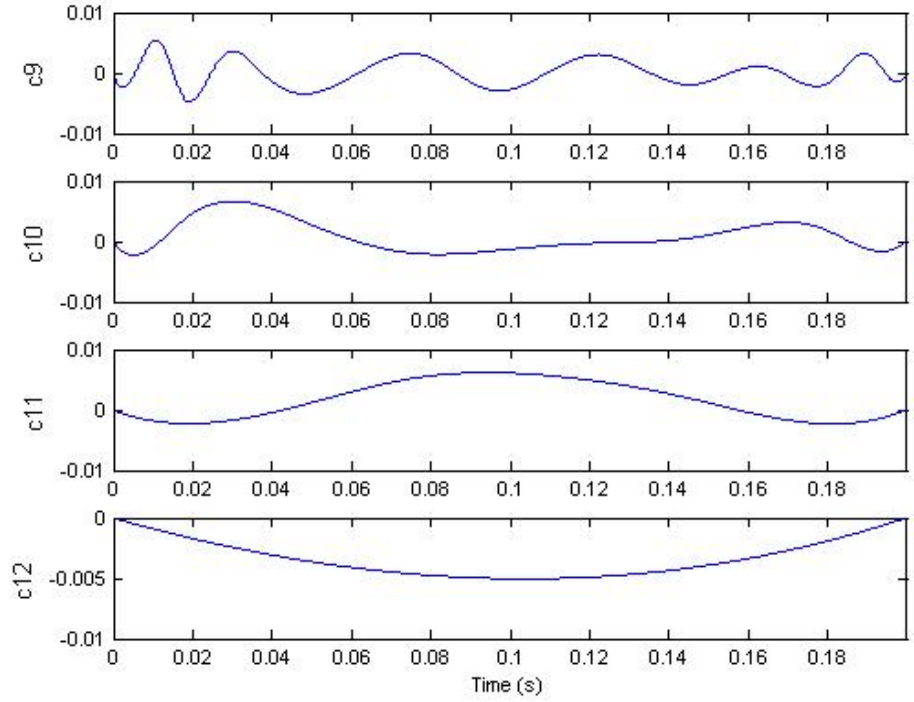

Figure 4.23: Water Steel 4.5 V 22.5 Hz IMF

4.2.5 Digital Particle Image Velocimetry

The following plots describe the velocity and vorticity field determined by the DPIV analysis. The velocity fields depict arrows varying in size proportional to the velocity of the fluid. The following plots were produced after the plates have been oscillating for a few minutes to ensure that the flow around the plate has reached a steady state.

The vorticity plots include contours of red and blue areas of varying shades correlating to the magnitude of vorticity. Each plot includes a positive clockwise flow and also a negative counterclockwise component of the flow. Table 4.2 lists the amount of circulation measured for each vortex ring shown in Figures 4.25, 4.27, and 4.29, with the nylon plate having the greatest amount of circulation. The numbers listed are for the vortices generated above (Top) and below (Bottom) the plane of the plate. As vortices are shed alternately above and below the plate, the magnitude of the circulation varies.

Table 4.2: Circulation of Selected Vortex Pairs

	Steel		Aluminum		Nylon		
Top	8.2	-9.2	11.7	-12	9.8	-10.4	cm^2/s
Bottom	12.9	-11.1	18	-17.9	24.6	-21.6	cm^2/s

The kinetic energy transferred from the plate to surrounding fluid can be calculated by use of equation 10. The mass m used is a unit mass of 1 cm^3 of water at 1000 kg/m^3, the velocity V is the velocity for a 1 cm^2 frame in m/s computed while producing the velocity plots.

$$KE_{frame} = \frac{mV^2}{2} \tag{10}$$

The value KE_{frame} is summed for the total number of N frames used in the experiment and the average taken, producing the average kinetic energy of the flow. The mean kinetic energy is then divided by the number of vortex pairs P present in the slide, to produce the mean fluid energy per vortex pair KE_{pair} as calculated using equation 11.

$$KE_{pair} = \frac{\sum_{j=1}^{N} KE_{frame,j}}{NP} \tag{11}$$

The calculated energies for a single vortex pair are listed in table 4.3. The nylon plate transferred the most energy to the surrounding fluid per vortex pair because it is the most flexible of the plates studied. This observation agrees with the findings of [11] where more flexible plates were able to transfer more energy from the flow.

Table 4.3: Mean Fluid Energy per Vortex Pair

	Steel	Aluminum	Nylon	
Mean	3.33E-02	2.86E-02	6.08E-02	Joule

Figure 4.24 shows the velocity field for the steel plate driven at 5 V and 15 Hz. The blue arrows indicate the direction and magnitude of the flow for the 1 cm^2 frame it is centered in. The flow is seen to travel perpendicular to the plate represented by the black line as the left end of the plate is the free end.

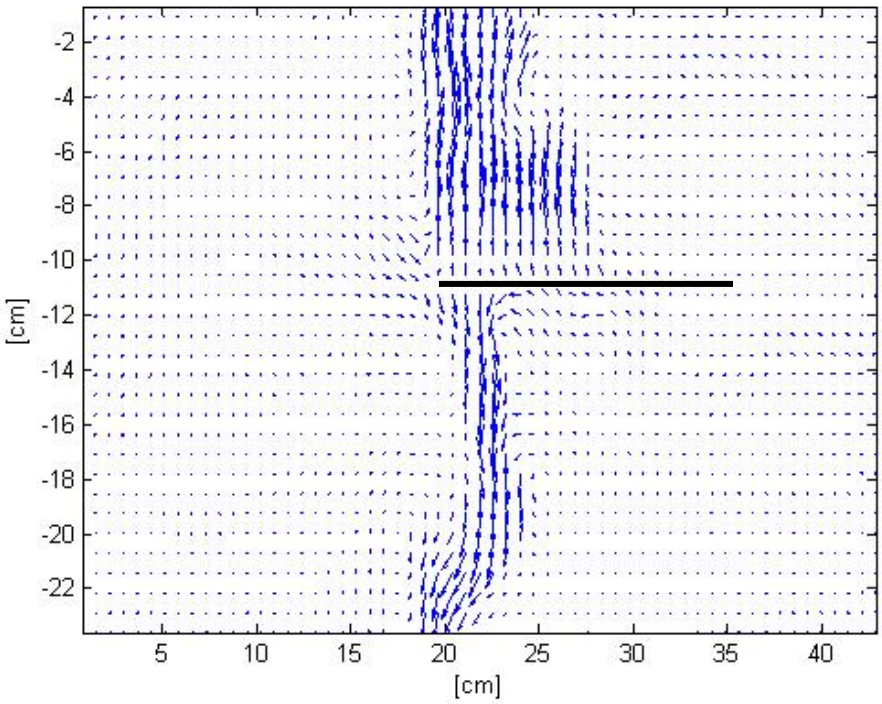

Figure 4.24: Water Steel 5 V 15 Hz Velocity Plot

Figure 4.25 depicts the vorticity plot for the steel plate. Vortex pairs can be seen above and below the plate. The velocity plot was able to capture the extent of the fluid flow, but was not able to clearly describe the points of clockwise or counterclockwise rotational flow. The plot for steel depicts vortex pairs in which the rings are very close together and of similar magnitude.

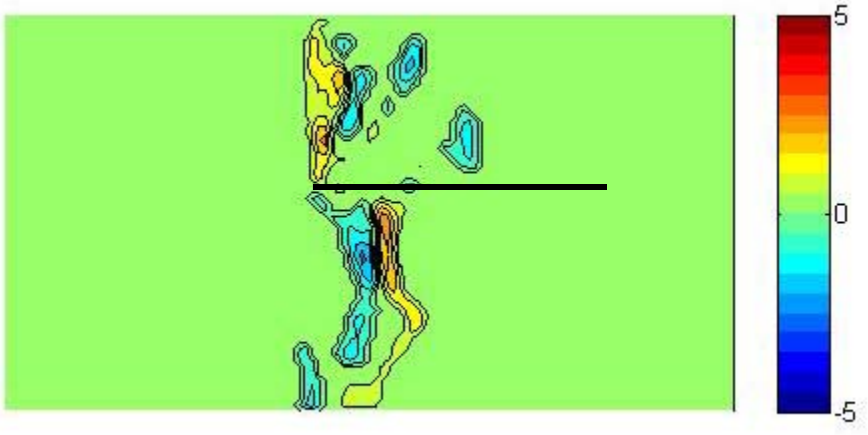

Figure 4.25: Water Steel 5 V 15 Hz Vorticity Plot

Figure 4.26 depicts the velocity field for the aluminum plate. The flow is seen to also be traveling vertically perpendicular to the free end of the plate. The velocity is slightly less than that of the steel plate.

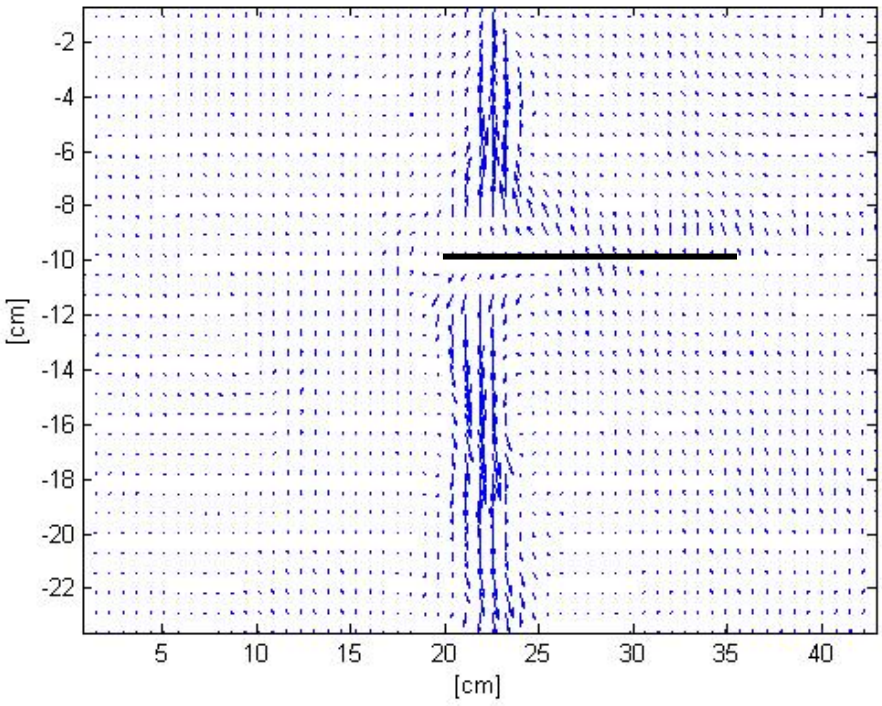

Figure 4.26: Water Aluminum 5 V 15 Hz Velocity Plot

Figure 4.27 depicts the vorticity plot for the aluminum plate showing contours of vorticity. The vortex pairs are very neatly traveling perpendicular to the plate with little disturbances from the existing flow field. The circulation for the vortex pairs are listed in Table 4.2.

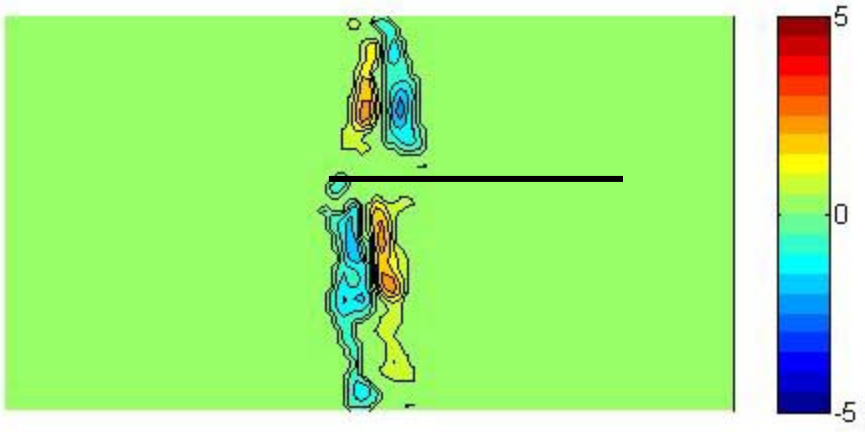

Figure 4.27: Water Aluminum 5 V 15 Hz Vorticity Plot

Figure 4.28 depicts a flow travelling at an angle to the free end of the plate. This may be due to the plate having a slight curve in it as a result of the manufacturing process.

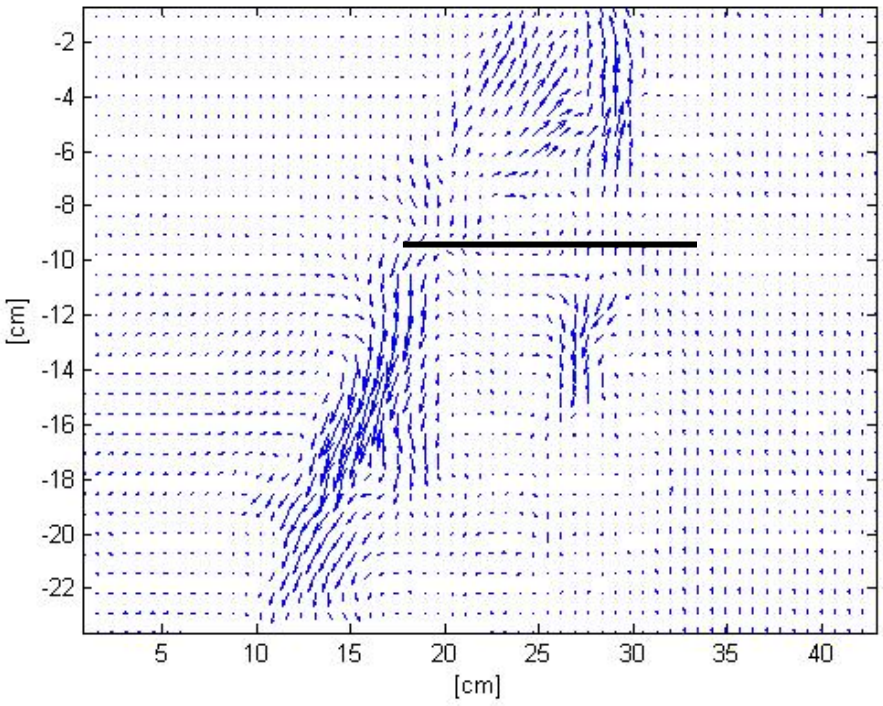

Figure 4.28: Water Nylon 5 V 15 Hz Velocity Plot

Figure 4.29 depicts the vorticity for the nylon plate with multiple vortex pairs present above and below the plate. The multiple pairs are from previous oscillation cycles which have been shed but have not yet left the field of view of the camera. The vortices produced from the nylon plate are smaller size but have greater amounts of vorticity at the center of each vortex.

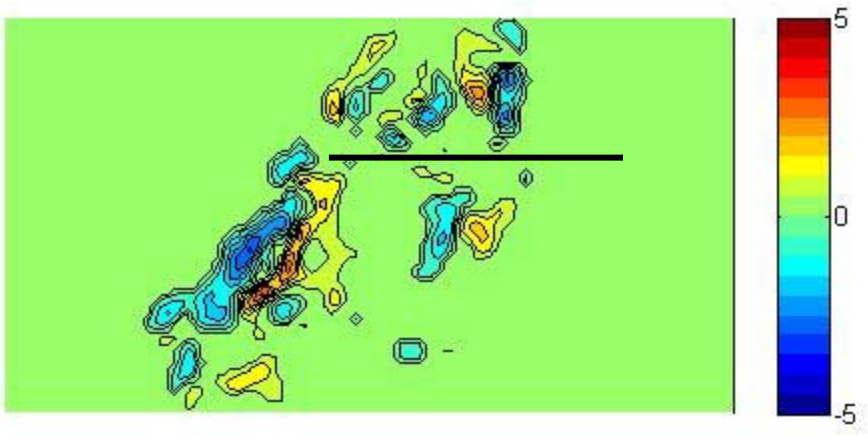

Figure 4.29: Water Nylon 5 V 15 Hz Vorticity Plot

Chapter 5 Conclusions

5.1 Conclusions

The response characteristics of forced vibrating plates of different materials were studied in air and water. The responses of the plates were compared by material as the plate was forced in the two different mediums at multiple combinations of amplitude and frequency. By use of Fourier and wavelet analysis, it is observed that the response frequencies for each plate material behaved slightly differently and provided only limited information on the response signal throughout the sampling period. The HHT was performed on the response of the plate for all materials and found to be a more detailed description of the response.

The most flexible plate was able to transfer the most energy to the surrounding fluid. Material selection and material properties were shown to have a great influence on the energy transferred from the plate to the surrounding fluid.

The present study has demonstrated the applicability of several signal analysis techniques for use in studying nonlinear vibrations. The HHT is an appropriate tool for analyzing coupled fluid-structure systems, and shows potential for cantilevered plates as a means of fluid-structure energy transfer.

References

[1] Lindholm, U. S., Kana, D. D., Chu, W. H., and Abramson H. N., 1965, "Elastic Vibration Characteristics of Cantilever Plates in Water," Journal of Ship Research, **9**, pp. 11-22.

[2] Fu, Y., and Price, W. G., 1987, "Interactions Between a Partially or Totally Immersed Vibrating Cantilever Plate and the Surrounding Fluid," Journal of Sound and Vibration, **118**(3), pp. 495-513.

[3] Keulegan, G. H., and Carpenter, L. H., 1958, "Forces on Cylinders and Plates in an Oscillating Fluid," Journal of Research of the National Bureau of Standards, **60**(5), pp. 423-440.

[4] Ergin, A., and Uğulu, B., 2003, "Linear Vibration Analysis of Cantilever Plates Partially Submerged in Fluid," Journal of Fluids and Structures, **17**, pp. 927-939.

[5] Liang, C. C., Liao, C. C., Tai, Y. S., and Lai, W. H., 2001, "The Free Vibration Analysis of Submerged Cantilever Plates," Ocean Engineering, **28**, pp. 1225-1245.

[6] Münch, C., Ausoni, P., Braun, O., Farhat, M., and Avellan, F., 2010, "Fluid-Structure Coupling for an Oscillating Hydrofoil," Journal of Fluids and Structures, **26**, pp. 1018-1033.

[7] Young, Y. L., Chae, E. J., and Akcabay, D. T., 2012, "Hybrid Algorithm for Modeling of Fluid-Structure Interaction in Incompressible, Viscous flows," Acta Mechanica Sinica, **28**(4), pp. 1030-1041.

[8] Klaka, K., Penrose, J. D., Horsley, R. R., and Renilson, M. R., 2007, "Hydrodynamic Tests on a Plate in Forced Oscillation," Ocean Engineering, **34**, pp. 1225-1234.

[9] Barannyk, O., Buckham, B. J., and Oshkai, P., 2012, "On Performance of an Oscillating Plate Underwater Propulsion system with Variable chordwise Flexibility at Different Depths of submergence," Journal of Fluids and Structures, **28**, pp. 152-166.

[10] Sarpkaya, T., 2004, "A critical review of the intrinsic nature of vortex-induced vibrations," Journal of Fluids and Structures, **19**, pp. 389-447.

[11] Tang, L., Païdoussis, M. P., and Jiang, J., 2009, "Cantilevered Flexible Plates in Axial Flow: Energy Transfer and the Concept of Flutter-Mill," Journal of Sound and Vibration, **326**, pp. 263-276.

[12] Beerends, R. J., ter Morsche, H. G., van den Berg, J.C., and van de Vrie, E.M., 2003, *Fourier and Laplace Transforms*. Cambridge University Press, Cambridge, UK, Chap. 3.

[13] Newland, D. E., 1993, *An introduction to Random Vibrations, Spectral and Wavelet Analysis*, 3rd ed., John Wiley & Sons, New York, pp. 295.

[14] Huang, N. E., and Attoh-Okine, N. O., eds. 2005, *The Hilbert-Huang Transform in Engineering*, CRC Press, Boca Raton, FL, Chap. 1.

[15] Tan, A, 2008, "Hilbert-Huang Transform," MATLAB Central File Exchange, Retrieved March 1, 2013, http://www.mathworks.com/matlabcentral/file exchange/19681-hilbert-huang-transform